Spatial soliton pairs of the vectorial Thirring model realized in a coherent atomic system via electromagnetically induced transparency

Hui-jun Li and Kun Zhang

Institute of Nonlinear Physics and Department of Physics, Zhejiang Normal University, Jinhua, Zhejiang 321004, China

(Received 25 February 2016; revised manuscript received 5 December 2016; published 20 January 2017)

We propose a scheme to realize a (2+1)-dimensional vectorial Thirring model in a coherent atomic system via electromagnetically induced transparency (EIT). We show that under EIT conditions the probe field envelopes obey coupled nonlinear Schrödinger equations, which are reduced to a Thirring model when system parameters are suitably chosen. We present spatial soliton-pair solutions exhibiting many interesting features, including controllability (i.e., the soliton property of one component can be adjusted by the propagation constant of another component in which the soliton remains unchanged), diversity (i.e., many different types of soliton-pair solutions can be found, including bright-bright, dark-bright, dark-dark, darklike-dark, dark-dipole, darklike-multidark, and high-dimensional bright-bright, dark-darklike soliton pairs), and stability. Furthermore, we demonstrate that the stability of soliton pairs in the system can be strengthened by adjusting the propagation constant. Comparing with previous studies, in addition to supporting much more stable (1+1)-dimensional and (2+1)-dimensional spatial soliton-pair solutions, the present scheme needs only a single atomic species and hence is easy to realize experimentally.

DOI: 10.1103/PhysRevA.95.013829

I. INTRODUCTION

Spatial optical solitons are the special wave packets appearing as a result of interplay between diffraction and nonlinearity. Their study is of special interest due to their rich nonlinear physics and important practical applications [1–5]. Generally, spatial optical solitons are produced in passive optical media. In order to avoid significant optical absorption, a very high light intensity is used to obtain enough nonlinearity for balancing the diffraction effect.

In recent years, much interest has focused on the highly resonant media via electromagnetically induced transparency (EIT) [6]. An EIT system possesses many striking features, including the suppression of optical absorption [7], a large reduction of group velocity [8], a giant enhancement of Kerr nonlinearity with very low power light field [9], and many adjustable parameters, such as the strength of the control field, detuning, and atomic density. So, there has been much research in theory and experiment, including ultraslow optical transmission and storage [10,11], the phase gate [12], the optical clock [13], efficient four-wave mixing [14], the bistable state [15], and high-dimensional spatiotemporal optical solitons [16]. In addition, due to the similarity between the light field transmission equation and the quantum Schrödinger equation, the EIT system is also used to simulate some quantum systems [17], such as Anderson's model [18,19], the parity-time symmetrical model [20–23], and so on.

Despite extensive discussion of the giant cross-phase modulation (XPM) and the related solitons in EIT media, its study has been restricted mainly to the coupled nonlinear Schrödinger equation (CNLSE) [24], such as for symbiotic solitons [25] and fermionic bright solitons [26]. There is hardly any discussion about the soliton pair that arises solely from the balance between diffraction and XPM without the contribution from self-phase modulation (SPM). Until recent years, holographic [27–29] and Thirring-type [30] solitons were proposed in photorefractive and atomic media, respectively. But there still exist self-interaction terms in the denominators of saturation nonlinearity, so the Thirring model, which was proposed for the first time by Thirring in quantum field theory [31], is the only model in which there are no terms other than XPM terms in the nonlinear terms. However, this model, which was realized by using the two species of a coherent atomic system, is asymmetrical, so there are some drawbacks, i.e., only (1+1)-dimensional bright-bright (BB) soliton pairs are discussed.

In the present article, we suggest a six-level scheme [32] to realize the Thirring model in a lifetime-broadened atomic gas based on the mechanism of EIT. Different from the two-species scheme [30], the scheme we suggest here is a single-species scheme. And due to the asymmetry of the Thirring model [30], the coefficients of XPM terms must be positive; however, in our scheme, the sign and the size of nonlinear coefficients can be adjusted by the energy level detuning, conveniently. So, we can realize four kinds of Thirring models. In addition, we also find some characteristics that are different from the results of traditional CNLSE. First, in the Thirring soliton pair, one soliton can be controlled by the propagation constant of another equation satisfied by another soliton which will remain unchanged; we call this phenomenon response interchange (RI). So, the soliton pairs may be used as the optical switch. Second, we not only find the BB, dark-bright (DB), dark-dark (DD), darklike-dark (DLD, composed of the darklike soliton and dark soliton), dark-darklike (DDL, composed of two darklike solitons), and dark-dipole soliton pairs in the different Thirring models, but we also obtain DB, DD, DLD, dark-dipole, and darklike-multidark (DLMD) soliton pairs in the same model in which the nonlinear coefficients have opposite signs. Finally, though the two-dimensional (2D) soliton pairs are unstable due to the inherent instability, the stable 2D BB and DDL soliton pairs are obtained by controlling the propagation constant. Compared with the scheme proposed by Segev's group [30], the advantages of our scheme are as follows:

(1) In the case of using the same (or less) laser fields, this model can be achieved by a single species of atom.

(2) Due to utilizing two polarization components of the probe field, their propagation equations are completely symmetrical, so there exist DD soliton pairs.

(3) Owing to the tunable coefficients of XPM terms, there are more multiform soliton pairs.

(4) Moreover, this model is a vectorial Thirring model.

The rest of the article is arranged as follows. Section II describes the model under study. Section III derives the Thirring model using the multiple-scales method. Section IV investigates various soliton pairs and their stability. The final section (Sec. V) contains a discussion and summary of the main results of our work.

II. MODEL

The model under consideration is ^{87}Rb atomic gas (see Fig. 1). A linearly polarized (LP) pulsed probe field with center frequency ω_p (half Rabi frequency Ω_{p1} for right-circularly polarized field σ_- and Ω_{p2} for left-circularly polarized field σ_+), which can be transformed into two beams of circularly polarized fields as shown in Fig. 1(b), two strong LP control fields with frequencies ω_{c1} (half Rabi frequency Ω_{c1}) and ω_{c2} (half Rabi frequency Ω_{c2}), respectively, form a six-state system as shown in Fig. 1(a). The electric fields can be written as $\mathbf{E} = [\mathbf{e}_{p+}\mathcal{E}_{p+} + \mathbf{e}_{p-}\mathcal{E}_{p-}]\exp[i(k_p z - \omega_p t)] + \mathbf{e}_{cn}\mathcal{E}_{cn}\exp[i(-k_{cn}z - \omega_{cn}t)] + \text{c.c.}$ $(n = 1,2)$, where $\mathbf{e}_l$ and $k_l(\mathcal{E}_l)$ are respectively the polarization unit vector in the lth direction and the wave number (envelope) of the lth field. The one-half Rabi frequencies of the probe and the control field are $\Omega_{p1} = (\mathbf{e}_{p-}\cdot\mathbf{p}_{03(25)})\mathcal{E}_{p-}/\hbar$, $\Omega_{p2} = (\mathbf{e}_{p+}\cdot\mathbf{p}_{04(15)})\mathcal{E}_{p+}/\hbar$, $\Omega_{c1} = (\mathbf{e}_{c1}\cdot\mathbf{p}_{13})\mathcal{E}_{c1}/\hbar$, and $\Omega_{c2} = (\mathbf{e}_{c2}\cdot\mathbf{p}_{24})\mathcal{E}_{c2}/\hbar$, where $\mathbf{p}_{ij}$ is the electric dipole matrix element associated with the transition from $|i\rangle$ to $|j\rangle$. Then the Hamiltonian in the interaction picture reads $\hat{H}_{\text{int}} = -\hbar\sum_{j=1}^{5}\Delta_j|j\rangle\langle j| - \hbar(\Omega_{p1}|3\rangle\langle 0| + \Omega_{p1}|5\rangle\langle 2| + \Omega_{p2}|4\rangle\langle 0| + \Omega_{p2}|5\rangle\langle 1| + \Omega_{c1}|3\rangle\langle 1| + \Omega_{c2}|4\rangle\langle 2| + \text{H.c.})$, where $\Delta_{3,4} = \omega_p - (\omega_{3,4} - \omega_0)$, $\Delta_{1,2} = \omega_p - \omega_c - (\omega_{1,2} - \omega_0)$, and $\Delta_5 = 2\omega_p - \omega_c - (\omega_5 - \omega_0)$ are the one-, two-, and three-photon detunings, respectively.

Under the rotating-wave approximation, the evolution equations for atomic amplitude A_j $(j = 1\text{–}5)$ can be written as

$$\left(i\frac{\partial}{\partial t} + d_1\right)A_1 + \Omega_{c1}^* A_3 + \Omega_{p2}^* A_5 = 0, \tag{1a}$$

$$\left(i\frac{\partial}{\partial t} + d_2\right)A_2 + \Omega_{c2}^* A_4 + \Omega_{p1}^* A_5 = 0, \tag{1b}$$

$$\left(i\frac{\partial}{\partial t} + d_3\right)A_3 + \Omega_{c1} A_1 + \Omega_{p1} A_0 = 0, \tag{1c}$$

$$\left(i\frac{\partial}{\partial t} + d_4\right)A_4 + \Omega_{c2} A_2 + \Omega_{p2} A_0 = 0, \tag{1d}$$

$$\left(i\frac{\partial}{\partial t} + d_5\right)A_5 + \Omega_{p2} A_1 + \Omega_{p1} A_2 = 0, \tag{1e}$$

with $\sum_{i=0}^{5}|A_i|^2 = 1$, where $d_j = \Delta_j + i\gamma_j$ and γ_j $(j = 1\text{–}5)$ is the decay rate of the state $|j\rangle$.

Under a slowly varying envelope approximation, the Maxwell equation of the probe field is reduced to

$$i\left(\frac{\partial}{\partial z} + \frac{1}{c}\frac{\partial}{\partial t}\right)\Omega_{p1} + \frac{c}{2\omega_p}\left(\frac{\partial^2}{\partial x^2} + \frac{\partial^2}{\partial y^2}\right)\Omega_{p1} + \kappa_{03}A_3 A_0^* + \kappa_{25}A_5 A_2^* = 0, \tag{2a}$$

$$i\left(\frac{\partial}{\partial z} + \frac{1}{c}\frac{\partial}{\partial t}\right)\Omega_{p2} + \frac{c}{2\omega_p}\left(\frac{\partial^2}{\partial x^2} + \frac{\partial^2}{\partial y^2}\right)\Omega_{p2} + \kappa_{04}A_4 A_0^* + \kappa_{15}A_5 A_1^* = 0, \tag{2b}$$

with $\kappa_{04,15} = N\omega_p|\mathbf{e}_{p+}\cdot\mathbf{p}_{04,15}|^2/(2\epsilon_0\hbar c)$, $\kappa_{03,25} = N\omega_p|\mathbf{e}_{p-}\cdot\mathbf{p}_{03,25}|^2/(2\epsilon_0\hbar c)$, where N is the atomic concentration. In the following, we assume that the time duration of the probe field is large enough so that the time dependence of the Rabi frequencies Ω_{p1} and Ω_{p2} can be neglected (i.e., continuous approximation).

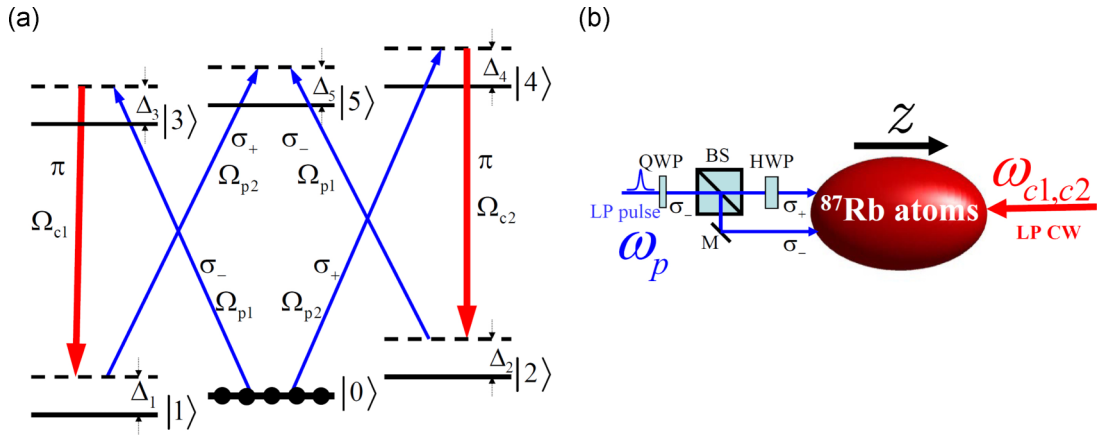

FIG. 1. (a) Excitation scheme of the lifetime broadened six-state atomic system interacting with a strong, continuous-wave control field with the half Rabi frequency Ω_{cn}, and a weak, linear polarized pulsed probe field with the half Rabi frequency Ω_{pn} $(n = 1,2)$. (b) Possible experimental arrangement of the laser fields, where ω_p and $\omega_{c1,c2}$ are the linearly polarized (LP) pulsed probe field and LP cw control fields, respectively. There is a 45° angle between the polarization direction of the LP pulse and the principle axis of the quarter-wave plate (QWP). BS and HWP are a 50:50 beam splitter and a half-wave plate, respectively. And σ^+ (σ^-) denotes the left (right)-circularly polarized laser field.

III. ASYMPTOTIC EXPANSION AND THE THIRRING MODEL

To solve the Maxwell Schrödinger equations (1) and (2), one employs the standard method of multiple scales. We assume that the atomic population whose loss is characterized by a small parameter ε is in the ground state $|0\rangle$ initially. The asymptotic expansions for the atomic amplitudes and probe field envelopes are $A_l = \sum_{j=0}^{\infty} \varepsilon^j A_l^{(j)}$ $(l = 0\text{–}5)$ and $\Omega_{pn} = \sum_{j=1}^{\infty} \varepsilon^j \Omega_{pn}^{(j)}$ $(n = 1,2)$. And the multiscale variables $z_l = \varepsilon^l z$ $(l = 0,2)$, $x_1 = \varepsilon x$, and $y_1 = \varepsilon y$ are introduced to avoid divergence. Substituting these expansions and the multiscale variables into Eqs. (1) and (2), we obtain a series of equations for $A_l^{(j)}$ and $\Omega_{pn}^{(j)}$ $(l = 0\text{–}5, n = 1,2)$, as shown in the Appendix.

At ε order, we obtain

$$\Omega_{pn}^{(1)} = F_n \exp(ik_n z_0), \quad n = 1,2, \tag{3}$$

with $k_{1,2} = \kappa_{03,04} d_{1,2}/D_{1,2} = \beta'_{1,2} + i\alpha_{1,2}$, $D_{1,2} = |\Omega_{c1,c2}|^2 - d_{1,2}d_{3,4}$, and F_n are the envelope functions depending on slow variables z_2, x_1, and y_1.

At ε^3 order, using the solvability conditions for $\Omega_{pn}^{(3)}$, we obtain the (2+1)-dimensional CNLSE:

$$i\frac{\partial F_n}{\partial z_2} + \frac{c}{2\omega_p}\left(\frac{\partial^2}{\partial x_1^2} + \frac{\partial^2}{\partial y_1^2}\right)F_n - (W_{n1}|F_1|^2 + W_{n2}|F_2|^2)F_n = 0, \tag{4}$$

with $W_{nn} = k_n G_n \exp(-2\alpha'_n z_2)$, $G_n = (|\Omega_{cn}|^2 + |d_n|^2)/|D_n|^2$, $\alpha'_n = \varepsilon^2 \alpha_n$, and $W_{12,21} = [k_{1,2}G_{2,1} + (\kappa_{25,15}\Omega_{c2,c1}/D_{2,1}^* + \kappa_{03,04}\Omega_{c1,c2}/D_{1,2})(\Omega_{c1}^*/D_1 + \Omega_{c2}^*/D_2)/d_5]\exp(-2\alpha'_{1,2}z_2)$.

At ε^2 and ε^3 orders, we have taken $\Omega_{pn}^{(2)} = \Omega_{pn}^{(3)} = 0$. Considering the asymptotic expansions, we know $\Omega_p = \varepsilon F \exp(ik_n z_0)$.

After returning to the original variables, the (2+1)-dimensional CNLSE (4) takes the dimensionless form

$$i\frac{\partial u_1}{\partial s} + \nabla_\perp^2 u_1 + \sigma_{11}|u_1|^2 u_1 + \sigma_{12}|u_2|^2 u_1 = 0, \tag{5a}$$

$$i\frac{\partial u_2}{\partial s} + \nabla_\perp^2 u_2 + \sigma_{21}|u_1|^2 u_2 + \sigma_{22}|u_2|^2 u_2 = 0, \tag{5b}$$

where $\nabla_\perp^2 = \frac{\partial^2}{\partial \xi^2} + \frac{\partial^2}{\partial \eta^2}$, $s = z/L_{\text{diff}}$, $\xi = x/R_x$, $\eta = y/R_y$, $u_n = \Omega_{pn}\exp(-ik_n z)/U_0$, and $\sigma_{mn} = -W_{mn}/|W_{12}|$ $(m,n = 1,2)$, with $L_{\text{diff}} = 2\omega_p R_x^2/c$ as the typical diffraction length, and we have taken the typical nonlinear length $L_{\text{NL}} = L_{\text{diff}} = 1/|W_{12}U_0^2|$, with $U_0 = \sqrt{c/(2\omega_p R_x^2|W_{12}|)}$ as the typical Rabi frequency of the probe field. Here, if $R_x = R_y$, this model is (2+1) dimensional; if $R_x \ll R_y$, the y-directional diffraction $\partial^2/\partial\eta^2$ can be neglected, so CNLSE (5) is reduced to being (1+1) dimensional.

For a practical example, we select the D_1 line transition $5^2S_{1/2} \rightarrow 5^2P_{1/2}$ and D_2 line transition $5^2S_{1/2} \rightarrow 5^2P_{3/2}$ of ^{87}Rb atoms, respectively.

We now make some remarks about how to design the Thirring model. In the first case, we construct the Thirring model in which the signs of XPM terms are the same by considering the D_1 line transition. The levels of the system are taken as $|0\rangle = |5S_{1/2}, F = 1, m_F = 0\rangle$, $|1\rangle = |5S_{1/2}, F = 1, m_F = -1\rangle$, $|2\rangle = |5S_{1/2}, F = 1, m_F = 1\rangle$, $|3\rangle = |5P_{1/2}, F = 1, m_F = -1\rangle$, $|4\rangle = |5P_{1/2}, F = 1, m_F = 1\rangle$, and $|5\rangle = |5P_{1/2}, F = 1, m_F = 0\rangle$. The parameters are $\gamma_0 = \Delta_0 = 0$, $2\gamma_1 = 2\gamma_2 = 300\ \text{s}^{-1}$, $2\gamma_3 = 2\gamma_4 = 2\gamma_5 = 3.6 \times 10^7\ \text{s}^{-1}$, $\omega_p = 2.37 \times 10^{15}\ \text{s}^{-1}$, and $R_x = 2.52 \times 10^{-3}$ cm [33].

According to the formulas below Eq. (4), if $k_n G_m$ $(n,m = 1,2)$ are small enough, then only XPM terms remain. Now, we make some reasonable assumptions and approximations:

(1) Use one beam of the control field; that is, $\Omega_{c1} = \Omega_{c2} = \Omega_c$.

(2) Consider the quantum interference conditions of EIT $|\Omega_c|^2 \gg |d_{1,2}d_{3,4}|$, and take $|\Omega_c|^2 \gg |d_n|^2$, $|\Omega_c|^2 \gg |d_n d_5|$, which ensures that SPM terms are far less than XPM terms. And the size and the sign of the XPM terms can be controlled by the detuning Δ_5.

(3) In the cases of $\kappa_{03} = \kappa_{25} = \kappa_1$ and $\kappa_{04} = \kappa_{15} = \kappa_2$, $W_{nn} \ll W_{12,21} \approx 4\kappa_{1,2}/(d_5|\Omega_c|^2)$; that is, $\sigma_{nn} \ll \sigma_{12,21}$, and $\sigma_{12,21}$ can be adjusted by $\kappa_{1,2}$.

We take $\Omega_c = 6.0 \times 10^7\ \text{s}^{-1}$, $\kappa_2/c_0 = \kappa_1 = 1.0 \times 10^{11}\ \text{cm}^{-1}\,\text{s}^{-1}$, $\Delta_1 = \Delta_2 = -3.0 \times 10^4\ \text{s}^{-1}$, $\Delta_3 = \Delta_4 = 3.0 \times 10^8\ \text{s}^{-1}$, and $\Delta_5 = \mp 1.5 \times 10^9\ \text{s}^{-1}$, in which c_0 is a free parameter that can be adjusted by the polarization direction of the electric dipole transition matrix elements. Substituting these parameters into the coefficient expressions of CNLSE (5), we can obtain the typical diffraction length $L_{\text{diff}} = 1.0$ cm, the typical Rabi frequency $U_0 = 3.67 \times 10^6\ \text{s}^{-1}$, and the absorption coefficient $\alpha_1 = \alpha_2/c_0 = 0.004\ \text{cm}^{-1}$, and these coefficients of the SPM and XPM terms are

$$\sigma_{11} = \sigma_{22}/c_0 = (3.1 - 0.015i) \times 10^{-3}, \tag{6a}$$

$$\sigma_{12} = \sigma_{21}/c_0 = \pm 1.0 + 0.01i. \tag{6b}$$

In the second case, we construct the Thirring model in which the signs of the XPM terms are arbitrary using the D_2 line transition. The levels of the system are taken as $|0\rangle = |5S_{1/2}, F = 2, m_F = 0\rangle$, $|1\rangle = |5S_{1/2}, F = 2, m_F = -1\rangle$, $|2\rangle = |5S_{1/2}, F = 2, m_F = 1\rangle$, $|3\rangle = |5P_{3/2}, F = 1, m_F = -1\rangle$, $|4\rangle = |5P_{3/2}, F = 3, m_F = 1\rangle$, and $|5\rangle = |5P_{3/2}, F = 2, m_F = 0\rangle$. The parameters are $\gamma_0 = \Delta_0 = 0$, $2\gamma_1 = 2\gamma_2 = 300\ \text{s}^{-1}$, $2\gamma_3 = 2\gamma_4 = 2\gamma_5 = 3.8 \times 10^7\ \text{s}^{-1}$, $\omega_p = 2.41 \times 10^{15}\ \text{s}^{-1}$, and $R_x = 2.52 \times 10^{-3}$ cm [33].

Through these formulas following Eq. (4), if $\kappa_{25,15} \ll \kappa_{03,04}$, $|\Omega_{c1,c2}|^2 \ll |d_{1,3}|^2$, and $|\Omega_{c2}|^2 \gg |d_2 d_4|$, then $W_{11,22}$, the second term of W_{12}, and the first term of W_{21} are all small, so we obtain $W_{12} \approx -\frac{\kappa_{03}}{d_3|\Omega_{c2}|^2}$, $W_{21} \approx \frac{\kappa_{04}}{d_5|\Omega_{c2}|^2}$. Therefore, the Thirring model can be realized by choosing suitable parameters, and the nonlinear signs can be controlled by the signs of the detunings $\Delta_{3,5}$ independently. The concrete parameters are $\Omega_{c1} = 5\Omega_{c2} = 6.0 \times 10^7\ \text{s}^{-1}$, $\kappa_{04}/c_0 = 5.1\kappa_{03} = 25.5\kappa_{15,25} = 2.55 \times 10^9\ \text{cm}^{-1}\,\text{s}^{-1}$, $\Delta_1 = \Delta_4 = 3.0 \times 10^8\ \text{s}^{-1}$, $\Delta_2 = 0$, and $\Delta_5 = \pm 5\Delta_3 = \mp 2.0 \times 10^9\ \text{s}^{-1}$, in which c_0 is a free parameter. Substituting all these parameters into the coefficient expressions of CNLSE (5), we can obtain the typical diffraction length $L_{\text{diff}} = 1.0$ cm, the typical Rabi frequency $U_0 = 9 \times 10^6\ \text{s}^{-1}$, and the absorption coefficient $\alpha_1 = 15\alpha_2/c_0 = 0.06\ \text{cm}^{-1}$; these coefficients of

SPM and XPM terms are

$$\sigma_{11} = (\pm 6.0 - 0.3i) \times 10^{-4},$$
$$\sigma_{22}/c_0 = (0.001 - 3.0i) \times 10^{-3}, \tag{7a}$$
$$\sigma_{12} = \pm 1.0 - 0.04i,$$
$$\sigma_{21}/c_0 = \pm 1.0 + 0.01i, \tag{7b}$$

when $\Delta_5 = -5\Delta_3 = \mp 2.0 \times 10^9 \mathrm{s}^{-1}$, and

$$\sigma_{11} = (\pm 6.0 - 0.3i) \times 10^{-4},$$
$$\sigma_{22}/c_0 = (0.001 - 3.0i) \times 10^{-3}, \tag{8a}$$
$$\sigma_{12} = \pm 1.0 - 0.04i,$$
$$\sigma_{21}/c_0 = \mp 1.0 + 0.01i, \tag{8b}$$

when $\Delta_5 = 5\Delta_3 = \pm 2.0 \times 10^9 \mathrm{s}^{-1}$.

According to these results, $\sigma_{11,22}$, $\alpha_{1,2}$, and the imaginary parts of $\sigma_{12,21}$ can be neglected. Therefore, Eq. (5) can be written as

$$i\frac{\partial u_1}{\partial s} + \nabla_\perp^2 u_1 + \sigma_1 |u_2|^2 u_1 = 0, \tag{9a}$$
$$i\frac{\partial u_2}{\partial s} + \nabla_\perp^2 u_2 + \sigma_2 c_0 |u_1|^2 u_2 = 0, \tag{9b}$$

where the size and sign of $\sigma_{1,2}$ ($\sigma_{1,2} = \sigma_{12,21}$) can be controlled by $\Delta_{3,5}$. Equation (9) is the (2+1)-dimensional Thirring model.

We successfully construct the Thirring model by using the coherent atomic medium with EIT effect. And in light of Eqs. (6)–(8), we can design four kinds of Thirring models. In this scheme, the model can be realized only by two (or three) beams of laser fields and single species of atoms. In Ref. [30], if the coupled equations are completely symmetric, SPM terms cannot be ignored. But in our system, even if Eq. (9) satisfied by two polarized components of the probe field is completely symmetric, SPM terms are still ignored safely. Furthermore, the size of the SPM terms can be adjusted by the detuning $\Delta_{1,2}$ conveniently, so we can also construct the Manakov model in our system.

IV. THE SOLITON-PAIR SOLUTIONS OF THE THIRRING MODEL

In this part, we discuss the soliton-pair solutions of Eq. (9) and their stability. We suppose $u_n = \psi_n(\xi,\eta)e^{-i\beta_n s}$ ($n = 1,2$), where β_n are the propagation constants. Then Eq. (9) becomes the coupled steady-state equations

$$\beta_1\psi_1 + \nabla_\perp^2\psi_1 + \sigma_1|\psi_2|^2\psi_1 = 0, \tag{10a}$$
$$\beta_2\psi_2 + \nabla_\perp^2\psi_2 + \sigma_2 c_0|\psi_1|^2\psi_2 = 0. \tag{10b}$$

By using the Newton conjugate gradient method, the profiles and power $P_n = \int_{-\infty}^{+\infty} |\psi_n|^2\, d\xi\, d\eta$ or the renormalized power $P_n - P_n^0 = |\int_{-\infty}^{+\infty}(|\psi_n|^2 - |\psi_n^0|^2)\, d\xi\, d\eta|$ (mainly for the soliton with background) of the soliton-pair solutions are obtained in the following sections; here ψ_n^0 is the amplitude of the background. Once the soliton-pair solutions ψ_n are obtained, one can analyze their linear stability by considering a perturbation to them, i.e.,

$$u_n = \{\psi_n + \varepsilon'[w_n(\xi,\eta)e^{-\lambda s} + v_n^*(\xi,\eta)e^{-\lambda^* s}]\}e^{-i\beta_n s} \quad (n = 1,2), \tag{11}$$

where w_n and v_n are the normal modes, and λ is the corresponding eigenvalue of the perturbation. Substituting Eq. (11) into Eq. (9), one obtains the following linear eigenvalue problem:

$$\begin{pmatrix} L_1 & 0 & \sigma_1\psi_1\psi_2^* & \sigma_1\psi_1\psi_2 \\ 0 & -L_1 & -\sigma_1\psi_1^*\psi_2^* & -\sigma_1\psi_1^*\psi_2 \\ c_0\sigma_2\psi_2\psi_1^* & c_0\sigma_2\psi_2\psi_1 & L_2 & 0 \\ -c_0\sigma_2\psi_1^*\psi_2^* & -c_0\sigma_2\psi_2^*\psi_1 & 0 & -L_2 \end{pmatrix} \begin{pmatrix} w_1 \\ v_1 \\ w_2 \\ v_2 \end{pmatrix} = i\lambda \begin{pmatrix} w_1 \\ v_1 \\ w_2 \\ v_2 \end{pmatrix}, \tag{12}$$

with $L_n = \beta_n + \nabla_\perp^2 + c_{0n}\sigma_n|\psi_{3-n}|^2$ ($n = 1,2$), $c_{01} = 1$, and $c_{02} = c_0$, which can be solved numerically by using the Fourier collocation method [34]. The soliton-pair solutions ψ_n are stable if the real parts of all the eigenvalues are positive or zero. We also prove their stability by the split-step Fourier propagation method.

A. The soliton-pair solutions for the (1+1)-dimensional Thirring model with $\sigma_1 = \sigma_2 = 1$

We now present the soliton-pair solutions of Eq. (10) with $\sigma_1 = \sigma_2 = 1$ and check their stability by using the numerical simulations. First, we show BB soliton-pair solutions of Eq. (10). Figure 2(a) shows the power curves which are the function of the propagation constant β_1 with $c_0 = 1$ and $\beta_2 = -0.49$. From Fig. 2(a), we find that when β_1 remains unchanged, the power of ψ_1 is close to constant with the propagation constant β_1 in most regions; however, the power of ψ_2 decreases gradually. This property can also be found by the profiles of $|\psi_{1,2}|$ in Figs. 2(b) and 2(c), in which the profiles of ψ_1 change a little, but the profiles of ψ_2 significantly change with β_1. Compared with the Manakov system (or CNLSE), in which the power and profiles will change with the propagation constant itself, the power and profile depend on the propagation constant of its cooperative partner in the Thirring model, which is called the RI phenomenon. This result can be used to design the optical switch. However, the RI phenomenon only exists in a part of the β_1 region, rather than the whole range as shown in Fig. 2(a). The reason for the RI phenomenon is that when one changes β_1 but β_2 remains unchanged as shown by the small circles in Fig. 2(a), this term $\sigma_1|\psi_2|^2 + \beta_1$ in Eq. (10a) can be regarded as an external potential, and the increasing of β_1 can be balanced by the decreasing peak value of ψ_2 for the remaining unchanged external potential, which ensures

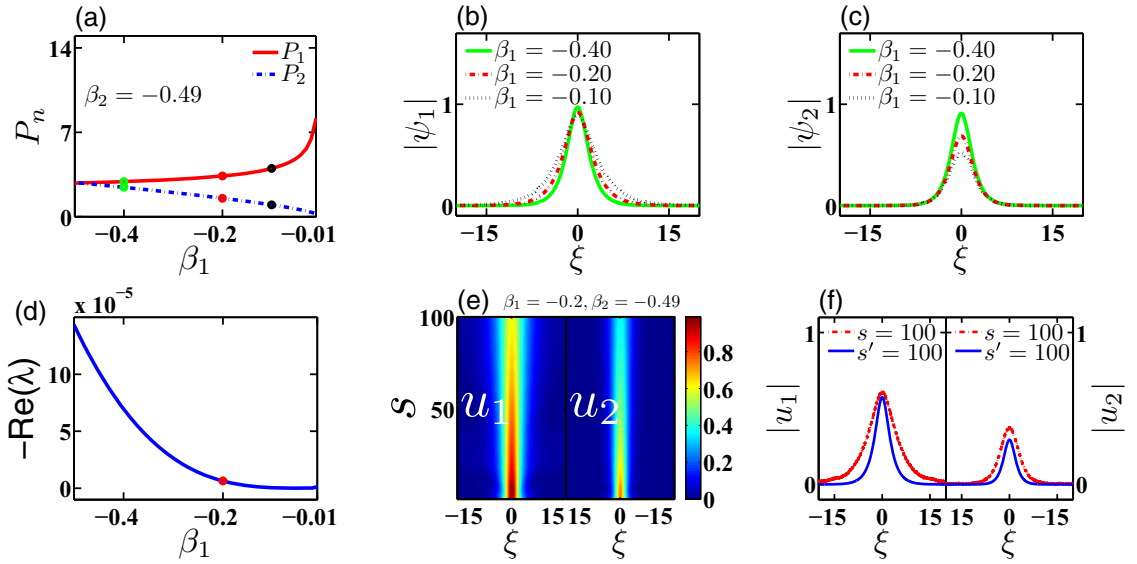

FIG. 2. (a) Power curves of BB soliton pairs with propagation constant β_1 ($\beta_2 = -0.49$). (b), (c) Profiles of BB soliton pairs with different propagation constant β_1, with corresponding parameters denoted by the small circles of (a), respectively. (d) Perturbation growth rate $-\mathrm{Re}(\lambda)$ with propagation constant β_1. (e) Propagations of BB soliton pair in the presence of the random perturbation by simulating Eq. (9) with the complex coefficients (6), with parameters denoted by the small circle of (d). (f) The comparison between the propagation results denoted by dot-dashed lines and the results of Eq. (13) denoted by solid lines. Here, $\sigma_1 = \sigma_2 = c_0 = 1$.

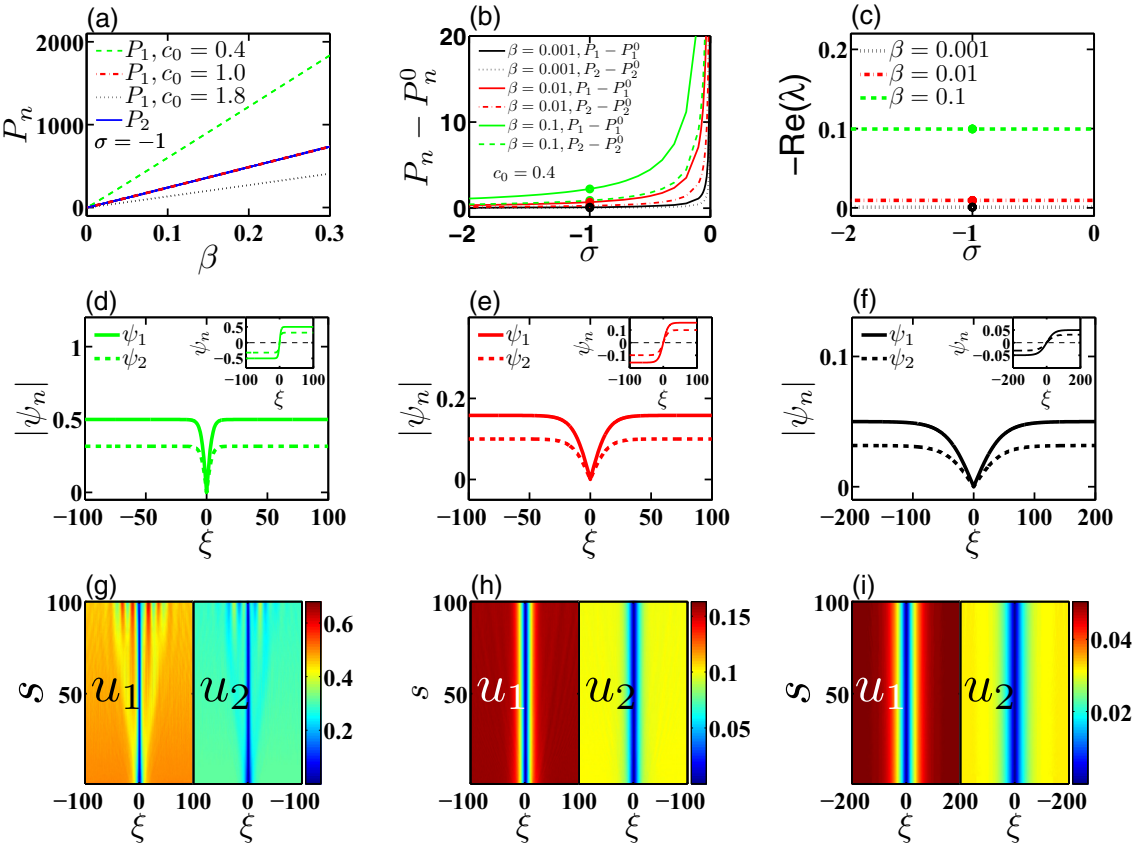

FIG. 3. (a) Power curves of DD soliton pairs with the propagation constant $\beta = \beta_{1,2}$ by taking $c_0 = 0.4, 1, 1.8$. (b) Power curves of DD soliton pairs with the nonlinear coefficients $\sigma = \sigma_{1,2}$ by taking the different propagation constants β; here $c_0 = 0.4$. (c) Perturbation growth rate $-\mathrm{Re}(\lambda)$ with the nonlinear coefficient σ by taking different propagation constant β. (d)–(f) Profiles of DD soliton pairs with different propagation constants which have been marked by the small circles in (b) and (c). (g)–(i) Propagations of DD soliton pairs shown in (d)–(f) in the presence of the random perturbation by simulating Eq. (9) with the complex coefficients (6).

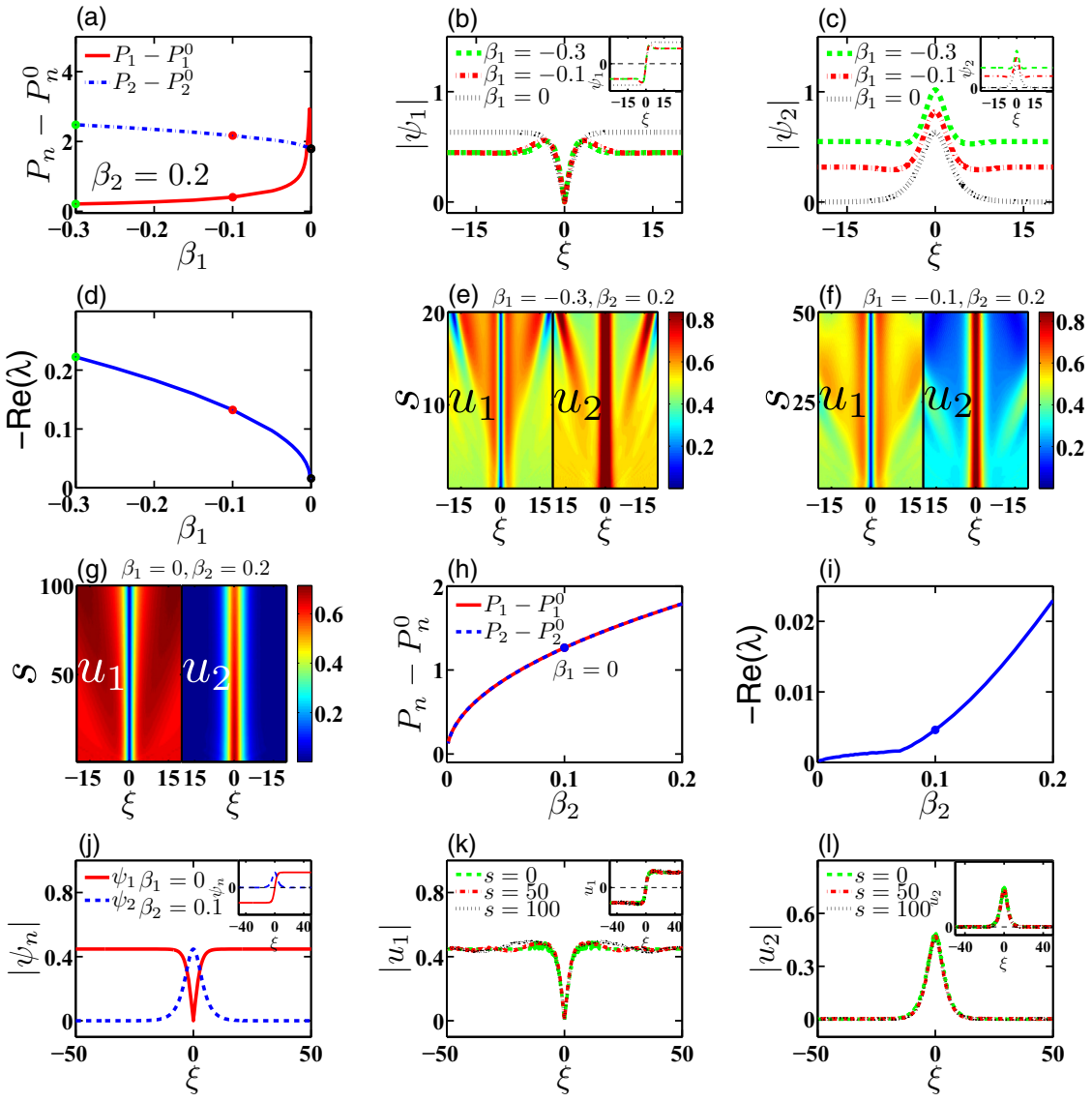

FIG. 4. (a) Power curves of DB soliton pairs with propagation constant β_1 ($\beta_2 = 0.2$) and (b), (c) for the profiles of DB soliton pairs with different β_1. (d) Perturbation growth rate $-\mathrm{Re}(\lambda)$ with the propagation constant β_1. (e)–(g) Propagations of DB soliton pairs. (h)–(l) Analogous results as shown in (a)–(g) with $\beta_1 = 0$. Here, $\sigma_1 = -\sigma_2 = c_0 = 1$.

the profile of ψ_1 is invariant in Eq. (10a). But with β_1 further increasing, we not only need to consider the contribution by the peak value of ψ_2, but also must take care of the profile of ψ_2 which will induce the change of the diffraction term $\partial^2\psi_1/\partial\xi^2$, so the profile of ψ_1 will change, which will result in the RI phenomenon being broken.

The stability of BB soliton pairs is checked by solving the eigenvalue problem (12). The eigenvalues are shown in Fig. 2(d). From the results, these soliton pairs are all stable. Furthermore, we make a numerical propagation on Eq. (9) with the complex coefficients (6) [these results are shown in Figs. 2(b) and 2(c) as the initial conditions] and, adding the random perturbations into them, i.e., we take $u_n(s = 0,\xi) = \psi_n(1 + \epsilon f)$, here $\epsilon = 0.1$, f is a random variable uniformly distributed in the interval $[0, 1]$. The evolution results are shown in Fig. 2(e), in which the peak values of the soliton pair decrease with the increasing propagation distance. The reason for the decaying amplitude is that there exist these imaginary parts in Eq. (9). By a rough approximation calculation, we obtain

$$u_1(s,\xi) \approx u_1(s = 0,\xi)\exp[i\sigma_1 \max(|u_2(s = 0,\xi)|^2)s], \tag{13a}$$

$$u_2(s,\xi) \approx u_2(s = 0,\xi)\exp[i\sigma_2 c_0 \max(|u_1(s = 0,\xi)|^2)s]. \tag{13b}$$

The comparison between the propagation result denoted by the dot-dashed lines and the approximation solution (13) denoted by the solid lines are shown in Fig. 2(f), from which we know the decay is caused mainly by the imaginary parts of Eq. (9). Though the attenuation of the amplitude is inevitable, the profile still remains after propagating for tens of centimeters.

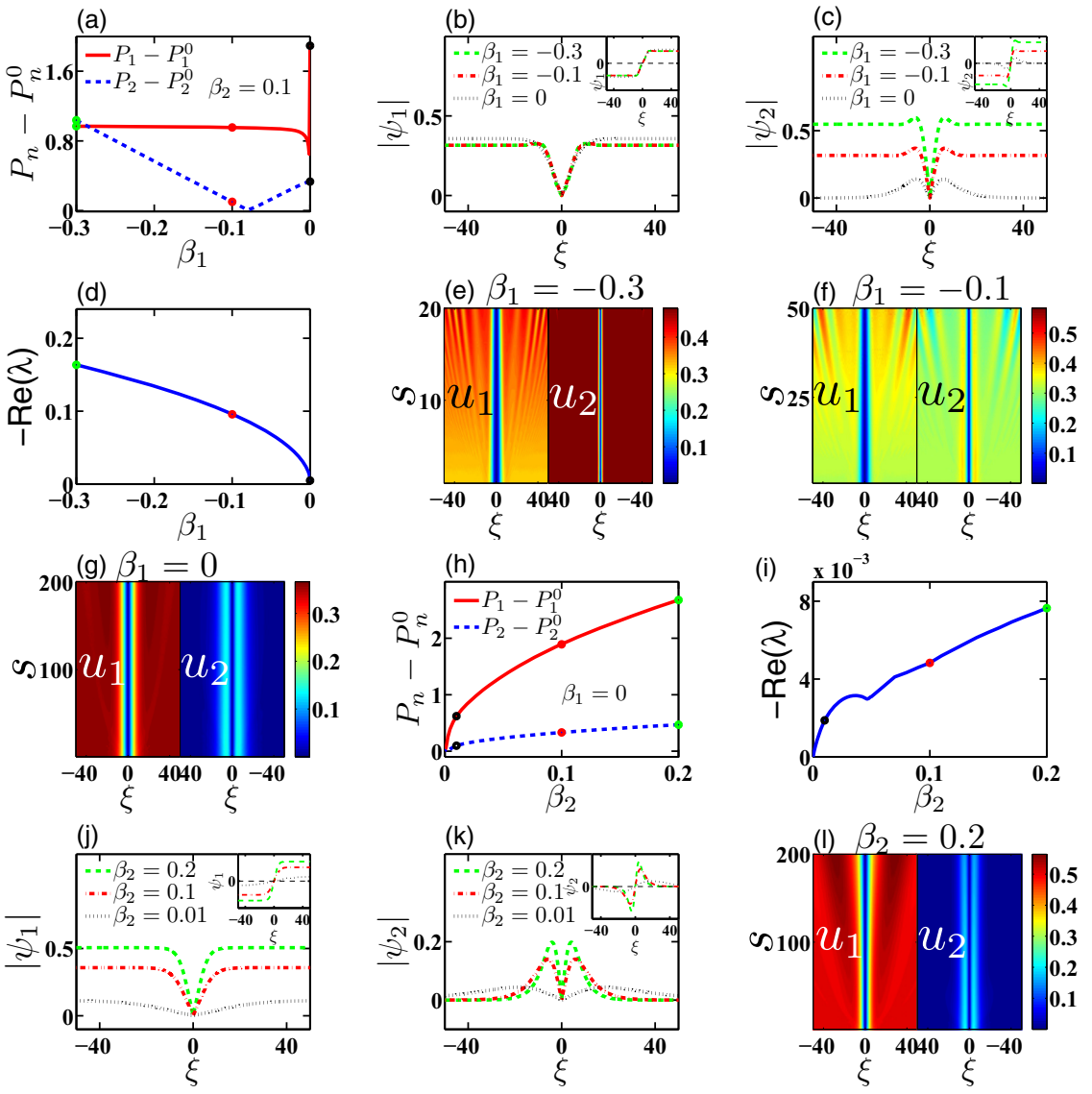

FIG. 5. (a) Power curves of DD soliton pairs with propagation constant β_1 ($\beta_2 = 0.1$) and (b), (c) for the profiles of DD soliton pairs with different β_1. (d) Perturbation growth rate $-\mathrm{Re}(\lambda)$ with the propagation constant β_1. (e)–(g) Propagations of DD soliton pairs marked by the circle in (a) and (d) with $\beta_2 = 0.1$. (h)–(l) Analogous results as shown in (a)–(g) with $\beta_1 = 0$. Here, $\sigma_1 = -\sigma_2 = c_0 = 1$.

B. The soliton-pair solutions for the (1+1)-dimensional Thirring model with $\sigma_1 = \sigma_2 = -1$

In this section, we find the soliton pair solutions of Eq. (10) with $\sigma_1 = \sigma_2 = -1$. Though there is no report about the solution for this kind of Thirring model, according to the experience about CNLSE, there exist DD soliton-pair solutions.

In Figs. 3(a) and 3(b), one shows the power curves of DD soliton pairs with the propagation constant $\beta_{1,2} = \beta$ by taking $c_0 = 0.4, 1, 1.8$ and the nonlinear coefficients $\sigma_{1,2} = \sigma$ with

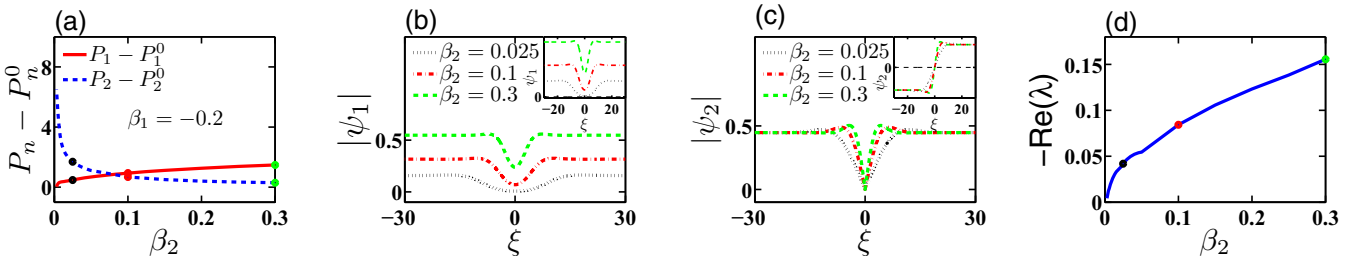

FIG. 6. (a) Power curves of DLD soliton pairs with propagation constant β_2 ($\beta_1 = -0.2$) and (b), (c) for the profiles of DLD soliton pairs with different β_2. (d) Perturbation growth rate $-\mathrm{Re}(\lambda)$ with the propagation constant β_2. Here, $\sigma_1 = -\sigma_2 = c_0 = 1$.

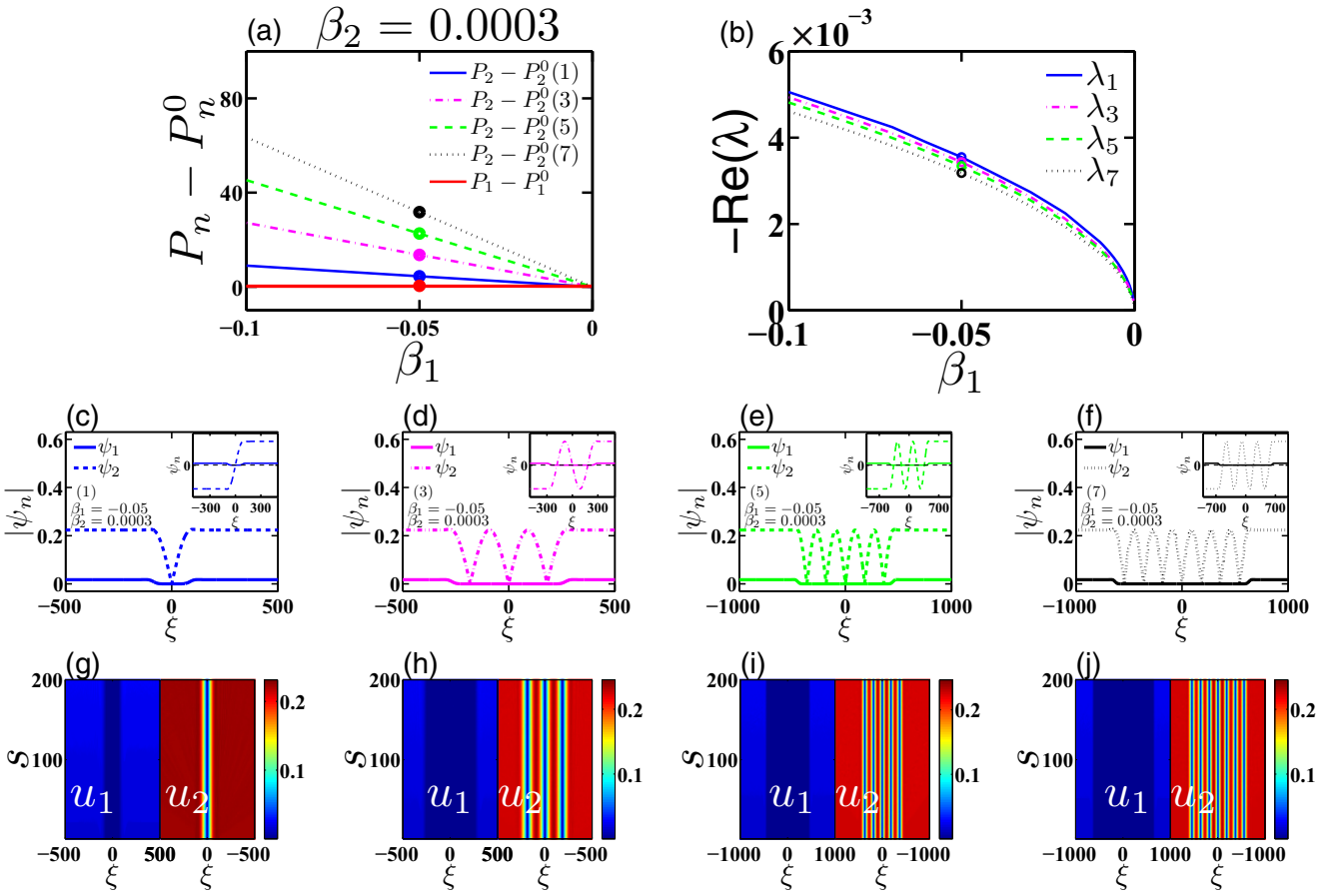

FIG. 7. (a) Power curves of DLMD soliton pairs with propagation constant β_1 ($\beta_2 = 0.1$). (b) Perturbation growth rate $-\mathrm{Re}(\lambda)$ with the propagation constant β_1. (c)–(f) The profiles for DLMD soliton pairs marked by the circle in (a) and (b) with the same β_1 and β_2. (g)–(j) Evolution results of DLMD soliton pairs in (c)–(f). Here, $\sigma_1 = -\sigma_2 = c_0 = 1$.

different propagation constant, respectively. In these figures, the results that the power of ψ_1 changes with c_0 at the same time that one of ψ_2 remains unchanged are quite counterintuitive and are also another evidence of RI. And we also find that the power is affected by the propagation constant and nonlinear coefficients in Fig. 3(b). But from Fig. 3(c), the stability of DD soliton pairs is not affected by nonlinear coefficients; it is only affected by the propagation constant. The smaller the propagation constant is, the more stable the soliton pairs become.

From the amplitudes $\psi_{1,2}$ in the insets of Figs. 3(d)–3(f), all dark solitons of soliton pairs are odd dark solitons which have an abrupt phase shift of π at their centers and are the antisymmetric function of space [35]. Taking the profiles in Figs. 3(d)–3(f) as the initial conditions, the corresponding propagation results are shown in Figs. 3(g)–3(i), respectively. Here, we have added the perturbation and considered the imaginary parts as the processing in Fig. 2(e). These propagation results further prove that DD soliton pairs become stable with decreasing propagation constant.

C. The soliton-pair solutions for the (1+1)-dimensional Thirring model with $\sigma_1 = -\sigma_2 = 1$

From the knowledge about the nonlinear Schrödinger equation (NLSE) or CNLSE, we know there are bright-dark soliton-pair solutions in the case of $\sigma_1 = -\sigma_2 = c_0 = 1$, but we only find the DB soliton-pair solutions for Eq. (10) as shown in Fig. 4. The reason is that one field feels the nonlinear trapping potential induced by another field, so the self-focusing or self-defocusing nonlinear effect in one equation will be identified by the nonlinear property in the equation of its cooperative partner. From Fig. 4(a), the power curves are shown. In Figs. 4(b) and 4(c), with the changing of β_1, the profiles of the DB soliton pairs are displayed. But the bright soliton is not the ground soliton when $\beta_1 \neq 0$; there is a uniform background. The background height of the bright soliton ψ_2 will decrease with the increasing of β_1, until ψ_2 becomes a ground soliton. We also analyze the stability of the DB soliton pair by numerical simulation. From the results of linear stability analysis in Fig. 4(d) and propagations in Figs. 4(e)–4(g), we find that the less $|\beta_1|$ becomes, the more stable the DB soliton pairs are. So, there are the stable soliton-pair solutions. The soliton pair for $\beta_1 = 0$ is unstable from Fig. 4(d), but it can steadily propagate for some distance as shown in Fig. 4(g) [about 100 cm, which far exceeds the size of our system (about several centimeters)]. In the case of $\beta_1 = 0$, the power curves in Fig. 4(h) and the stability curves in Fig. 4(i) with the propagation constant β_2 are shown. We find the bright soliton components of DB soliton pairs will degenerate into the ground soliton as shown in Fig. 4(j), and

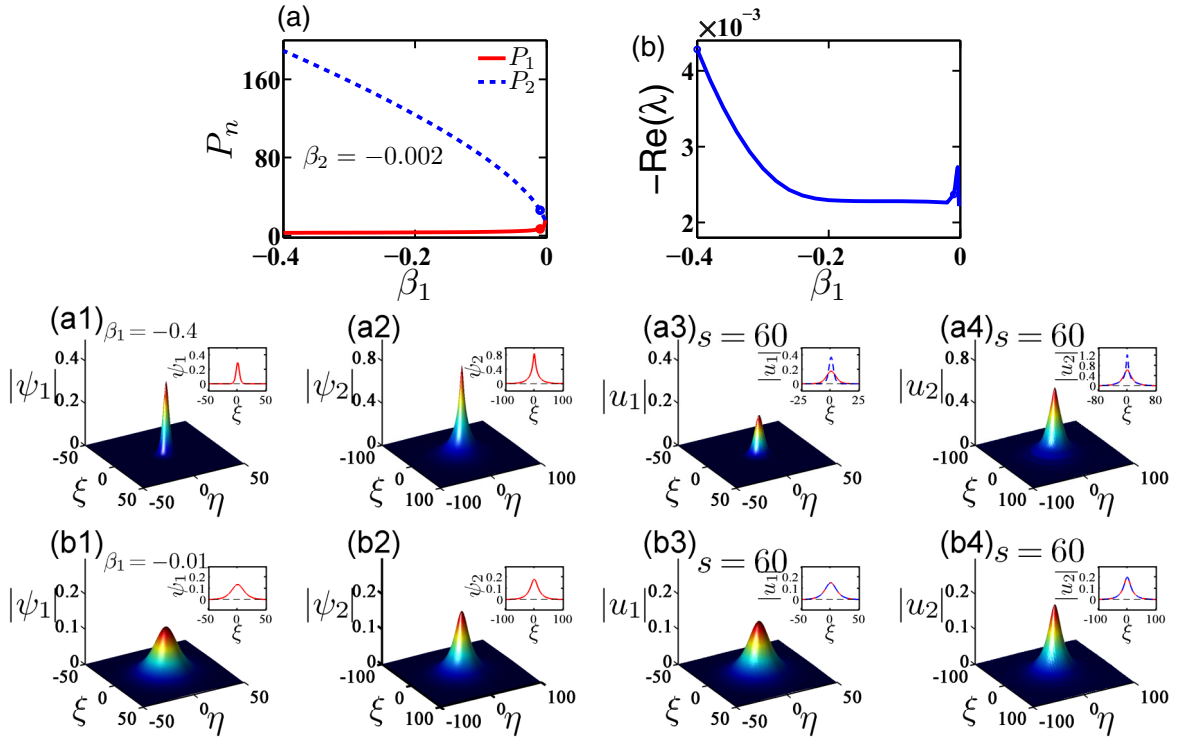

FIG. 8. (a) Power curves of BB soliton pairs with propagation constant β_1 ($\beta_2 = -0.002$). (b) Perturbation growth rate $-\mathrm{Re}(\lambda)$ with the propagation constant β_1. (a1)–(a4) The profiles and evolutions of BB soliton pairs with $\beta_1 = -0.4$. (b1)–(b4) The profiles and evolutions of BB soliton pairs with $\beta_1 = -0.01$. All these insets show the profiles by taking $\eta = 0$. The dashed lines in the insets denote the propagation results without considering the imaginary parts of Eq. (9). Here, $\sigma_1 = \sigma_2 = c_0 = 1$.

they will become more stable by the linear stability analysis result in Fig. 4(i) and the propagating results in Figs. 4(k) and 4(l).

Are there other solutions for Eq. (10) with $\sigma_1 = -\sigma_2 = 1$? By further numerical calculation, we find many soliton pairs.

In Fig. 5, we find DD and dark-dipole soliton-pair solutions. Through the power curves in Fig. 5(a), the RI property becomes more apparent. From the profiles in Figs. 5(b) and 5(c), with the increasing of β_1, the background height of ψ_2 decreases and that of ψ_1 almost remains unchanged, and the soliton pairs tend to be stable as shown in Figs. 5(d)–5(g).

In the case of $\beta_1 = 0$, we also present the power curves in Fig. 5(h) and stability curves in Fig. 5(i). From the profiles figures, we find the DD soliton pairs will degenerate into the dark-dipole soliton pair as shown in Figs. 5(j) and 5(k), and from Figs. 5(i) and 5(l), all these dark-dipole soliton pairs are stable; even the imaginary parts of nonlinear coefficients appear. These results tell us that DD soliton pairs can transform into dark-dipole soliton pairs by adjusting the propagation constant.

We also discover another type of soliton pair composed by a darklike soliton and a dark soliton (called DLD soliton pair) for Eq. (10) in Fig. 6. In Fig. 6(a), the power curves are shown. Compared with the dark solitons shown in Figs. 3–5, the profiles of ψ_1 are not the odd (or kink-type) dark solitons because there is no phase jump in its center but rather it is an even darklike soliton as shown in Fig. 6(b), in which we also find the intensity at the center decreases with the decreasing of β_2 until zero. Of course, the profiles of ψ_2 are still the kink-type dark soliton as shown in Fig. 6(c). The kink-type dark soliton is also called a black soliton [36]. This kind of DLD soliton pair is unstable from Fig. 6(d). For finding the stable soliton pairs, we further decrease the propagation constants $|\beta_1|$ and β_2.

Reducing β_2 to 0.0003, we obtain the soliton pairs which comprise the odd dark soliton and even darklike soliton in Fig. 7. In Fig. 7(a), the power curves of DLD and DLMD soliton pairs are shown, and we find the RI property still remains. From Fig. 7(b), these soliton pairs are all stable. The profiles for the darklike-single-dark soliton pair in Fig. 7(c), for the darklike-ternary-dark soliton pair in Fig. 7(d), for the darklike-quinary-dark soliton pair in Fig. 7(e), and for the darklike-septenary-dark soliton pair in Fig. 7(f) are obtained. There are one, three, five, and seven dips in the profile of $|\psi_2|$, respectively. Furthermore, the numerical propagation shown in Figs. 7(g)–7(j) is addressed, and we prove that all these DLMD soliton pairs are stable again. The reason is that ψ_1 provides a trapping potential for ψ_2.

D. The soliton-pair solutions for the (2+1)-dimensional Thirring model

It is well known that the solitons of the high-dimensional NLSE are generally unstable. Is there any chance to obtain high-dimensional soliton pairs with longer lifetime in the Thirring model? There has been no report on the study of high-dimensional spatial optical soliton pairs in the Thirring model except for the remark that the 2D Thirring BB soliton pairs suffer from a weak instability [30].

We find BB soliton pair solutions for the (2+1)-dimensional Thirring model (10) with $\sigma_1 = c_0 = \sigma_2 = 1$ in Fig. 8. From the power curves and stability curves, the stability will be

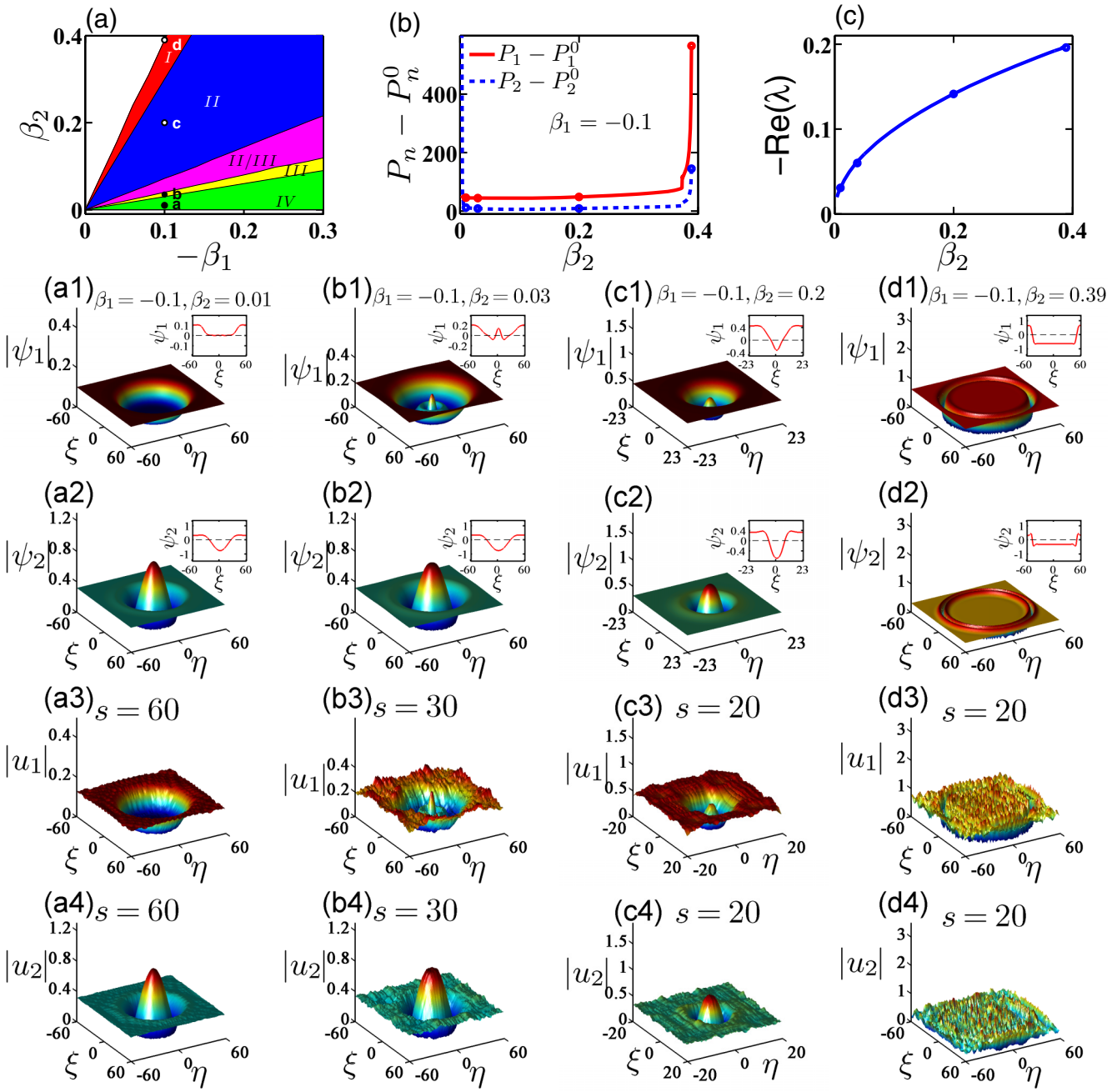

FIG. 9. (a) The existence domain of four types of DDL soliton pairs in the space of propagation constants β_1 and β_2. (b) Power curves of DDL soliton pairs with propagation constant β_2 ($\beta_1 = -0.1$). (b) Perturbation growth rate $-\mathrm{Re}(\lambda)$ with the propagation constant β_2. (a1)–(a4), (b1)–(b4), (c1)–(c4), and (d1)–(d4) show the profiles and evolution results of four kinds of DDL soliton pairs, respectively. Here, $\sigma_1 = -\sigma_2 = c_0 = 1$.

strengthened with the increasing of β_1 when $\beta_2 = -0.002$. After propagating $s = 60$ with a small randomness in the initial profiles u_n ($n = 1, 2$) and the small imaginary parts in the nonlinear coefficients of Eq. (9), the soliton pairs will broaden in the transverse direction when $\beta_1 = -0.4$, as shown in Figs. 8(a3) and 8(a4). However, when $\beta_1 = -0.01$, the effect of the small imaginary part disappears, and the profiles and amplitudes of the BB soliton pair remain unchanged after propagating 60 cm as shown in Figs. 8(b3) and 8(b4). Though the $-\mathrm{Re}(\lambda)$ is not equal to zero, we think the stability is enough to experimentally realize and observe.

To seek out the more stable high-dimensional soliton-pair solutions for the (2+1)-dimensional Thirring model (10), we choose $\sigma_1 = -\sigma_2 = c_0 = 1$. With the changing of the propagation constants $\beta_{1,2}$, there are different types of soliton pairs composed by two darklike solitons. To show the detail of the soliton existence intervals, the phase diagram of soliton types is shown in Fig. 9(a). Here, we define the existence ranges of four kinds of DDL soliton pairs which comprise the different types of darklike solitons. Then the power curves in Fig. 9(b) and stability curves in Fig. 9(c) are shown. Through the stability curves and propagating results in

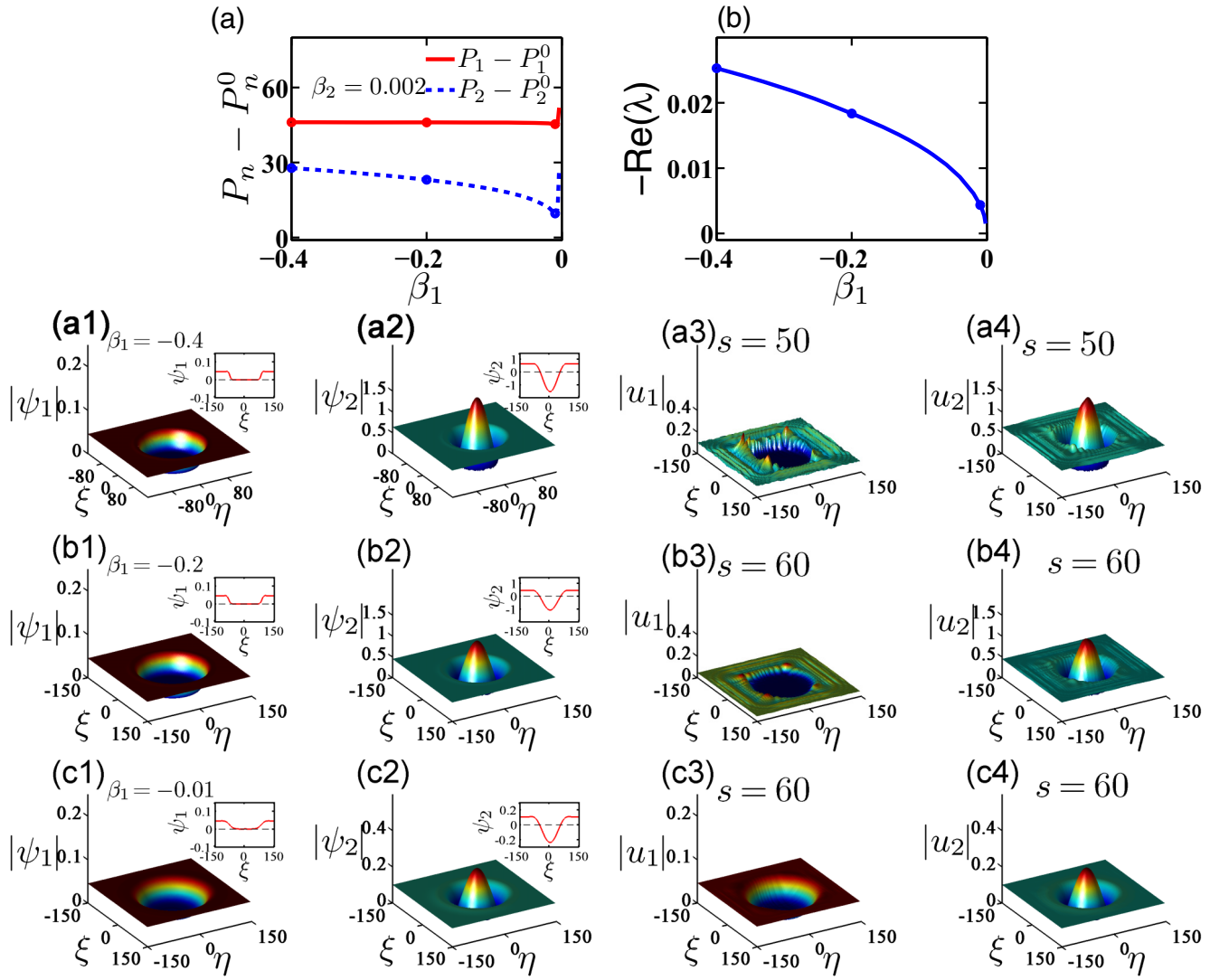

FIG. 10. (a) Power curves of DDL soliton pairs with propagation constant β_1 ($\beta_2 = 0.002$). (b) Perturbation growth rate $-\mathrm{Re}(\lambda)$ with the propagation constant β_1. (a1)–(a4), (b1)–(b4), and (c1)–(c4) show the profiles and evolution results of DDL soliton pairs with different propagation constant β_1, respectively. Here, $\sigma_1 = -\sigma_2 = c_0 = 1$.

Figs. 9(a3), 9(a4), 9(b3), 9(b4), 9(c3), 9(c4), 9(d3), and 9(d4), all these soliton pairs are unstable. But such soliton pairs as shown in Figs. 9(a1), 9(a2), 9(b1), 9(b2), 9(c1), 9(c2), 9(d1), and 9(d2) are also worth reporting.

To stabilize these DDL soliton pairs, we reduce β_2 to 0.002, and the power curves with the RI characteristic are shown in Fig. 10(a). In Fig. 10(b), we know that the stability will be strengthened with the increasing of β_1. In this case, there is only one kind of DDL soliton pair as shown in Figs. 10(a1), 10(a2), 10(b1), 10(b2), 10(c1), and 10(c2). To further prove the stability of the soliton pair, we make the numerical propagation as above. By these propagation results in Figs. 10(a3), 10(a4), 10(b3), 10(b4), 10(c3), and 10(c4), the soliton pairs for $\beta_1 = -0.01$ remain unchanged after propagating 60 cm. We think the stability is enough to experimentally realize and observe such a 2D DDL soliton pair for the Thirring model (10).

Compared with the unstable high-dimensional soliton in the NLSE or CNLSE, the reason for the high-dimensional Thirring-type BB and DDL soliton pairs being stable is that each soliton can provide an effective trapping potential for its cooperative partner; in particular, the darklike soliton trapped by this type of "even" darklike soliton in Fig. 9(a1) or Figs. 10(a1), 10(b1), and 10(c1) is more stable.

V. CONCLUSION AND SUMMARY

In this article, we have constructed a (2+1)-dimensional vectorial Thirring model satisfied by two polarized components of a probe field via EIT. The system we consider is a cold, resonant atomic gas having a six-level configuration and interacting with the probe and control fields. In this scheme, we only need one species of atom and two (or three) beams of laser fields. The constructed Thirring model is completely symmetric and has tunable nonlinear coefficients; that is, we can design four kinds of Thirring models. Based on these models, we have also discussed their soliton-pair solutions and their

stability. The nonlinear potentials are provided by XPM terms, so there are many distinctive properties. We not only discover the RI property of soliton pairs for the Thirring model which can be used to design all optical switching devices, but also find many kinds of stable soliton pairs, i.e., DB soliton pairs and DLMD soliton pairs in the same Thirring model. In addition, we also obtain the stable high-dimensional soliton pair for the (2+1)-dimensional Thirring model. All in all, the less the absolute value of propagation constant is, the more stable the corresponding soliton pairs are. All these properties point to the potential application of Thirring-type solitons for optical communication systems and optical processing systems.

ACKNOWLEDGMENTS

This project was supported by the National Natural Science Foundation of China (Grants No. 11204274 and No. 11574274), and the Natural Science Foundation of Zhejiang Province of China (Grants No. LY15A040002 and No. LZ15A050001).

APPENDIX: EQUATIONS IN SEC. III

These equations for $A_l^{(j)}$ and $\Omega_{pn}^{(j)}$ ($l = 0$–5, $n = 1,2$) are given by

$$d_1 A_1^{(j)} + \Omega_{c1}^* A_3^{(j)} = M_{(j)}, \quad M_1 = 0, \quad M_2 = 0, \quad M_3 = -\Omega_{p2}^{*(1)} A_5^{(2)}, \tag{A1a}$$

$$d_2 A_2^{(j)} + \Omega_{c2}^* A_4^{(j)} = N_{(j)}, \quad N_1 = 0, \quad N_2 = 0, \quad N_3 = -\Omega_{p1}^{*(1)} A_5^{(2)}, \tag{A1b}$$

$$d_3 A_3^{(j)} + \Omega_{c1} A_1^{(j)} + \Omega_{p1}^{(j)} = O_{(j)}, \quad O_1 = 0, \quad O_2 = 0, \quad O_3 = -\Omega_{p1}^{(1)} A_0^{(2)}, \tag{A1c}$$

$$d_4 A_4^{(j)} + \Omega_{c2} A_2^{(j)} + \Omega_{p2}^{(j)} = P_{(j)}, \quad P_1 = 0, \quad P_2 = 0, \quad P_3 = -\Omega_{p2}^{(1)} A_0^{(2)}, \tag{A1d}$$

$$A_5^{(2)} = \frac{1}{d_5}\left(\Omega_{p2}^{(1)} A_1^{(1)} + \Omega_{p1}^{(1)} A_2^{(1)}\right), \tag{A1e}$$

$$A_0^{(1)} = 0, \quad A_0^{(2)} = -\tfrac{1}{2}\left(\left|A_1^{(1)}\right|^2 + \left|A_2^{(1)}\right|^2 + \left|A_3^{(1)}\right|^2 + \left|A_4^{(1)}\right|^2\right), \tag{A1f}$$

$$i\frac{\partial}{\partial z_0}\Omega_{p1}^{(j)} + \kappa_{03} A_3^{(j)} = Q_{(j)}, \quad Q_1 = 0, \quad Q_2 = 0,$$

$$Q_3 = -i\frac{\partial}{\partial z_2}\Omega_{p1}^{(1)} - \frac{c}{2\omega_p}\left(\frac{\partial^2}{\partial x_1^2} + \frac{\partial^2}{\partial y_1^2}\right)\Omega_{p1}^{(1)} - \kappa_{03} A_3^{(1)} A_0^{*(2)} - \kappa_{25} A_5^{(2)} A_2^{*(1)}, \tag{A1g}$$

$$i\frac{\partial}{\partial z_0}\Omega_{p2}^{(j)} + \kappa_{04} A_4^{(j)} = R_{(j)}, \quad R_1 = 0, \quad R_2 = 0,$$

$$R_3 = -i\frac{l\partial}{\partial z_2}\Omega_{p2}^{(1)} - \frac{c}{2\omega_p}\left(\frac{\partial^2}{\partial x_1^2} + \frac{\partial^2}{\partial y_1^2}\right)\Omega_{p2}^{(1)} - \kappa_{04} A_4^{(1)} A_0^{*(2)} - \kappa_{15} A_5^{(2)} A_1^{*(1)}. \tag{A1h}$$

[1] G. I. Stegeman and M. Segev, Science **286**, 1518 (1999).
[2] Y. S. Kivshar and G. P. Agrawal, *Optical Solitons: From Fibers to Photonic Crystals* (Academic Press, New York, 2003).
[3] Y. F. Chen, K. Beckwitt, F. W. Wise, and B. A. Malomed, Phys. Rev. E **70**, 046610 (2004).
[4] B. A. Malomed, D. Mihalache, F. Wise, and L. Torner, J. Phys. B: Quantum Semiclass. Opt. **7**, R53 (2005).
[5] M. J. Paz-Alonso and H. Michinel, Phys. Rev. Lett. **94**, 093901 (2005).
[6] S. E. Harris, J. E. Field, and A. Imamoğlu, Phys. Rev. Lett. **64**, 1107 (1990).
[7] S. E. Harris, Phys. Today **50**, 36 (1997).
[8] L. V. Hau, S. E. Harris, Z. Dutton, and C. H. Behroozi, Nature (London) **397**, 594 (1999).
[9] H. Schmidt and A. Imamoğlu, Opt. Lett. **21**, 1936 (1996).
[10] D. F. Phillips, A. Fleischhauer, A. Mair, R. L. Walsworth, and M. D. Lukin, Phys. Rev. Lett. **86**, 783 (2001).
[11] Z. Chen, Z. Bai, H.-j. Li, C. Hang, and G. Huang, Sci. Rep. **5**, 8211 (2015).
[12] D. Petrosyan and M. Fleischhauer, Phys. Rev. Lett. **100**, 170501 (2008).
[13] R. Santra, E. Arimondo, T. Ido, C. H. Greene, and J. Ye, Phys. Rev. Lett. **94**, 173002 (2005).
[14] Y. Zhang, A. W. Brown, and M. Xiao, Phys. Rev. Lett. **99**, 123603 (2007).
[15] A. Joshi and M. Xiao, J. Mod. Opt. **57**, 1196 (2010).
[16] H.-j. Li, Y.-p. Wu, and G. Huang, Phys. Rev. A **84**, 033816 (2011).
[17] L. Stegano, Laser Photon. Rev. **3**, 243 (2009).
[18] J. Cheng and G. Huang, Phys. Rev. A **83**, 053847 (2011).
[19] H.-j. Li, J.-p. Dou, and G. Huang, Phys. Rev. A **89**, 033843 (2014).
[20] C. Hang, G. Huang, and V. V. Konotop, Phys. Rev. Lett. **110**, 083604 (2013).
[21] H.-j. Li, J.-p. Dou, and G. Huang, Opt. Express **21**, 32053 (2013).
[22] J. Sheng, M. A. Miri, D. N. Christodoulides, and M. Xiao, Phys. Rev. A **88**, 041803(R) (2013).

[23] J. Sheng, J. Wang, M. A. Miri, D. N. Christodoulides, and M. Xiao, Opt. Express **23**, 19777 (2015).
[24] S. K. Adhikari, Phys. Lett. A **346**, 179 (2005).
[25] V. M. Pérez-García and J. B. Beitia, Phys. Rev. A **72**, 033620 (2005).
[26] S. K. Adhikari, Phys. Rev. A **72**, 053608 (2005).
[27] O. Cohen, T. Carmon, M. Segev, and S. Odoulov, Opt. Lett. **27**, 2031 (2002).
[28] J. R. Salgueiro, A. A. Sukhorukov, and Y. S. Kivshar, Opt. Lett. **28**, 1457 (2003).
[29] O. Cohen, M. M. Murnane, and H. C. Kapteyn, Opt. Lett. **31**, 954 (2006).
[30] I. Friedler, G. Kurizki, O. Cohen, and M. Segev, Opt. Lett. **30**, 3374 (2005).
[31] W. Thirring, Ann. Phys. **3**, 91 (1958).
[32] D. Petrosyan and G. Kurizki, Phys. Rev. A **65**, 033833 (2002).
[33] D. A. Steck, Rubidium 87 D Line Data, http://steck.us/alkalidata/
[34] J. Yang, *Nonlinear Waves in Integrable and Nonintegrable Systems* (Society for Industrial and Applied Mathematics, Philadelphia, 2011).
[35] S. Baluschev, A. Dreischuh, I. Velchev, S. Dinev, and O. Marazov, Phys. Rev. E **52**, 5517 (1995).
[36] G. P. Agrawal, *Nonlinear Fiber Optics* (Academic Press, Singapore, 2009).